Extended lifespan and improved genome stability in HepaRG-derived cell lines through reprogramming by high-density stress

Charlotte Brun, Coralie Allain, Pierre-Jean Ferron,, Haifaou Younoussa, Bruno Colicchio, Éric Jeandidier, Radhia M'kacher, Christiane Guguen-Guillouzo, Fabrice Bertile

PNAS RESEARCH ARTICLE | CELL BIOLOGY

Extended lifespan and improved genome stability in HepaRG-derived cell lines through reprogramming by high-density stress

Charlotte Brun[a,b], Coralie Allain[c], Pierre-Jean Ferron[c], Haifaou Younoussa[d], Bruno Colicchio[e], Eric Jeandidier[f], Radhia M'Kacher[d], Christiane Guguen-Guillouzo[c], and Fabrice Bertile[a,b,1]

Edited by James Cleaver, University of California, San Francisco, CA; received November 11, 2022; accepted July 26, 2023

The characteristics and fate of cancer cells partly depend on their environmental stiffness, i.e., the local mechanical cues they face. HepaRG progenitors are liver carcinoma cells exhibiting transdifferentiation properties; however, the underlying mechanisms remain unknown. To evaluate the impact of external physical forces mimicking the tumor microenvironment, we seeded them at very high density for 20 h, keeping the cells round and unanchored to the substrate. Applied without corticoids, spatial confinement due to very high density induced reprogramming of HepaRG cells into stable replicative stem-like cells after replating at normal density. Redifferentiation of these stem-like cells into cells very similar to the original HepaRG cells was then achieved using the same stress but in the presence of corticoids. This demonstrates that the cells retained the memory required to run the complete hepatic differentiation program, after bypassing the Hayflick limit twice. We show that physical stress improved chromosome quality and genomic stability, through greater efficiency of DNA repair and restoration of telomerase activity, thus enabling cells to escape progression to a more aggressive cancer state. We also show the primary importance of high-density seeding, possibly triggering compressive stress, in these processes, rather than that of cell roundness or intracellular tensional signals. The HepaRG-derived lines established here considerably extend the lifespan and availability of this surrogate cell system for mature human hepatocytes. External physical stress is a promising way to create a variety of cell lines, and it paves the way for the development of strategies to improve cancer prognosis.

hepatocarcinoma | spatial confinement | stemness | telomere dynamics | DNA repair

Significance

Recent research highlights the key role of physical constraints and mechanotransduction in controlling cell differentiation and epigenetic memory. We show that very high-density seeding, possibly triggering compressive stress under spatial confinement, with or without corticoids, can direct the transdifferentiation of hepatoma HepaRG cells, establishing stable cell lines with enhanced genomic stability, delayed progression to a more aggressive cancer state, and no loss of epigenetic memory of the liver phenotype. By inducing a rejuvenation-like process that reprograms cells toward pluripotency through chromatin remodeling, resetting of DNA repair capacity and telomerase reactivation, our protocol opens avenues to perpetuate worldwide access to HepaRG cells and to design protective therapies to circumvent the problem of genomic instability associated with aggressive cancer phenotypes.

Hepatocellular carcinoma (HCC) is the most common primary malignant tumor in liver cancers, accounting for approximately 90% of cases (1, 2). A molecular classification of human HCC has been achieved, which distinguishes an aggressive and poorly differentiated proliferation class and a more differentiated nonproliferation class expressing numerous hepatocyte-like features and carrying a better prognosis (3, 4). Among the mutations that may lead to tumor transformation, those in the telomerase (*TERT*) promoter and in cellular tumor antigen p53 (*TP53*) and β-catenin (*CTNNB1*) genes have been identified as the most frequent in HCC (5). Other HCC subclasses result either from dedifferentiation of hepatic differentiated cells to hepatoblasts or to liver stem cells with not only self-renewal properties but also an ability for reprogramming toward differentiated tumors (6, 7). However, how these specific processes are triggered remains poorly understood, and their molecular bases have not been deciphered yet.

Tumor progression depends on modulation of the epigenome due to many factors present in the microenvironment, mainly those favoring fibrotic features, those preserving the characteristics of epithelioid cells, those contributing to the maintenance of a pool of stem cells involved in tumor reinitiation (8), and those influencing the number of cell divisions before reaching replicative senescence, known as the Hayflick limit (9). In fact, mechanostimulation and chemical stimuli are able to jointly control cell and tissue function (10), and physical forces in the tumor microenvironment shape the fate of cancer cells (11). A distinction is made between two types of forces that have a broad impact on cell fate: intracellularly generated forces, which produce mechanical tension on the matrix, and external forces produced by the environment that are applied from the outside onto the cells, including, for example, compression, hydrostatic pressure, or shear stress (12–15). Several pathways transduce mechanical signals from the periphery to the nucleus, including through Rho-kinase-dependent cytoskeletal dynamics, thereby triggering chromatin remodeling and reprogramming of gene expression (16).

Author contributions: C.G.-G. and F.B. designed research; C.B., C.A., P.-J.F., H.Y., B.C., E.J., R.M., C.G.-G., and F.B. performed research; C.B., R.M., C.G.-G., and F.B. analyzed data; and C.B., R.M., C.G.-G., and F.B. wrote the paper.

The authors declare no competing interest.

This article is a PNAS Direct Submission.

[1]To whom correspondence may be addressed. Email: fbertile@unistra.fr.

This article contains supporting information online at https://www.pnas.org/lookup/suppl/doi:10.1073/pnas.2219298120/-/DCSupplemental.

Published August 28, 2023.

Histological analysis of tumor fragments often shows abnormally high cellularity at the sites of active proliferation of cell nodules (7) since expanding tumors are often surrounded by a basement membrane that restricts the space in which the tumor can grow. The external physical forces involved in such cellular confinement contribute to locally increase the stiffness of the whole tissue, and changes in gene/protein expressions are ultimately triggered. Arrest of cell proliferation by space constraints has been reported, implying competition between cells for space and a key role for cell cycle regulators (17). One would expect such changes to promote the emergence or maintenance of a stem cell pool through dedifferentiation and reinitiation of differentiation and proliferation processes (18). Indeed, the dedifferentiation of adipocytes and more recently myofibroblasts has already been reported in response to compression (19, 20). It has also been shown that a single physical parameter, the distortion or roundness of the cells for example, can control the switch from one cell fate to another (21). A similar observation is made due to the replacement of one cell by another through mechanical cell competition processes (22). However, an experimentally validated signature of liver carcinoma cells linking, for example, gene/protein expression to dedifferentiation or reinitiation of differentiation under conditions of increased physical stress is still lacking. In addition, whether and how physical stress influences genomic stability is largely unknown.

The HepaRG cell system, which is known as a robust surrogate for primary human hepatocytes, has been reported to undergo a complete program of differentiation, including expression of many liver-specific genes/proteins (23). The tumor from which the HepaRG cell line was derived is an example of differentiated HCC with the characteristics of a typical mixed hepato-cholangiocarcinoma, minimally invasive because of lacking the three main mutations listed above (24, 25). Interestingly, HepaRG cells retained these noninvasive HCC properties, up to 18 passages (24). Like normal hepatocytes, they also retained their sensitivity to cell density in the presence of corticoids, a crucial property that contributes to the preservation of their polarized polygonal shape and capacity to fully differentiate when at confluence in vitro (26–29) or in spheroid conditions (30). In addition, HepaRG cells have dedifferentiation properties, and their evolution through a transient progenitor stage is characterized by the expression of specific progenitor markers at each passage during the proliferation phase (31). However, after 18 to 20 passages, progression through the transformation process worsens with the appearance of many defects, mainly the loss of cell polarity and of the ability to differentiate (32). This behavior of HepaRG cells resembles that of many cell types that enter replicative senescence after a limited number of divisions or population doublings (PDs) but can escape it by promoting cancer progression (33). Conversely, replicative senescence may delay the onset of transformation, thereby providing an important anticancer mechanism (34). Until now, these processes have never been studied in HepaRG cells.

The aim of this study was to decipher the responses of HepaRG cells to external forces possibly involving compression due to spatial confinement after seeding at very high density. From a combination of cell imaging and quantitative proteomics analysis, our data highlight mechanostimulation-induced cellular and molecular events, including those that reflect stem-like features and hepatic differentiation status of the established cell lines and the triggering epigenetic-related mechanisms that involve stress regulators and chromatin remodeling. These mechanisms ultimately influenced the replicative senescence–dependent number of cell divisions in the established cell lines. Detailed karyotyping and the analysis of DNA repair properties and telomere dynamics further demonstrated how external physical forces enhance chromosome quality and ultimately restore the number of cell divisions in a rejuvenation-like process—i.e., through reprogramming cells toward pluripotency. This study therefore lays the cellular and molecular foundations for how high-density seeding, possibly triggering compressive stress, drives transdifferentiation processes and genome stability in liver carcinoma.

Results and Discussion

Very High Density Is Sensed by HepaRG Cells and Allows Producing Cell Lines with Stable Proliferation. In order to determine how HepaRG liver progenitor cells detect physical and hormonal changes in their local microenvironment and transduce them into the nucleus to regulate gene expression, we implemented a strategy combining physical stress with or without corticoids and analyzed the resulting spatiotemporal cellular dynamics at different levels. A fundamental observation of our strategy was that seeding HepaRG progenitors at high density (2.15×10^5 cells/cm^2) to reach confluence directly leads to earlier engagement of cells in the differentiation program compared to low-density seeding. Indeed, the pluripotency marker OCT4 appears less abundant in this case from day 3, whereas the opposite is observed for markers of differentiated cells such as cytochrome P450 3A4 (CYP3A4) and F-actin (*SI Appendix*, Fig. S1*A*). Moreover, early after seeding (day 1), the expression of genes associated with hepatocyte differentiation (*HNF4a, Alb*) but also early development (*Oct4, Sox17, hTERT*) tends to be higher (1.5- to 2-fold and 2- to 9-fold, respectively) with high-density seeding (*SI Appendix*, Fig. S1*B*). This raised the question of the entry into differentiation of the cells via a possible transient reversion process toward a stem state. To better understand such undescribed processes in HepaRG cells, the challenge was therefore to create conditions that could stabilize the stem state and delay differentiation. For 20 h, we prevented the cells from anchoring and spreading, thus avoiding any internal tension force on the matrix, but we created space constraints by seeding at very high density (vHD, 4.3×10^5 cells/cm^2), a process that had the advantage of preserving contacts between neighboring cells, a key parameter of the local microenvironment (21). After these first 20 h in a corticoid-free medium, the cells were replated in controlled conditions of spreading and proliferation (2.7×10^4 cells/cm^2), which allowed the establishment of a stable cell line that we named HepaSL (Fig. 1*A* and *SI Appendix*, Fig. S2*A*). Here, at passage 4, HepaSL cells exhibited the morphology of typical epithelio-mesenchymal cells, similar to HepaRG progenitors at day 3 postseeding (*SI Appendix*, Fig. S2 *B* and *C*). However, their behavior was changed regarding lifespan and differentiation properties, as they acquired a great potential for self-renewal/cell expansion. Indeed, the 20-h spatial confinement due to very high density was applied to HepaRG cells at passage 13 (41.6 PDs), with these cells at risk of escaping to the transformation process after only about 22.4 additional PDs due to their estimated maximum cell division capacity of 64 PDs (32). The cells of the stem-like HepaSL line were found to be able to reach a total of about 66 PDs (i.e., 20 new passages) before entering a phase of functional instability and transformation (*SI Appendix*, Figs. S2*A* and S3*A*). Thus, here, we witness an extension of the expansion capacity of HepaRG cells, which is found to be restored by the establishment of the HepaSL cell line (*SI Appendix*, Figs. S2 *A* and *B* and S3*A*). To better characterize HepaSL cells, we tested their ability to fully differentiate in response to endocrine signals, as human embryonic stem cells (ESCs) do (35). Sequentially, we exposed proliferative HepaSL cells at passage 4 to activin A, FGF2, and BMP4, then to activin A alone, and then to the TGFb1

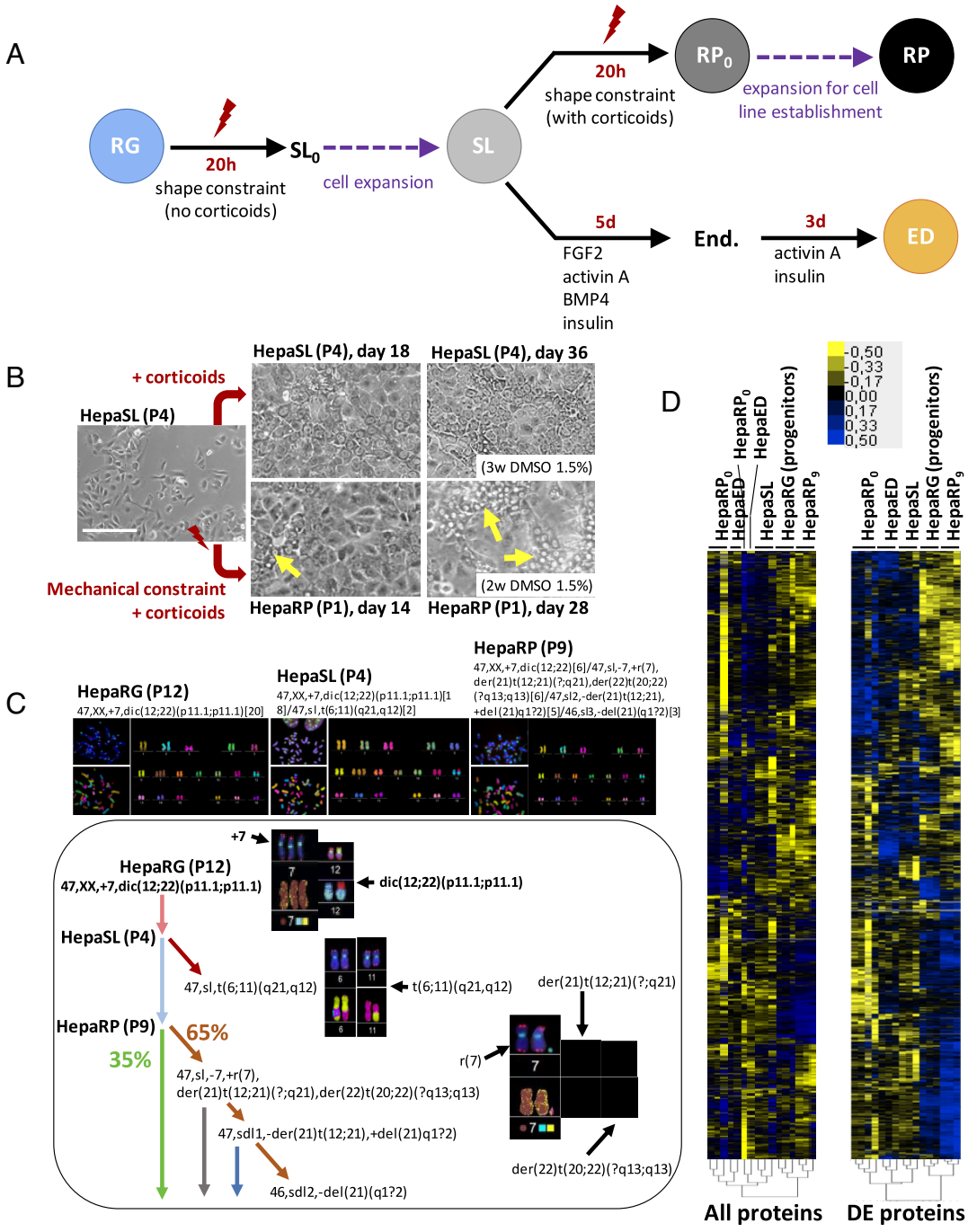

Fig. 1. Study design and main features of HepaRG and HepaRG-derived cell lines. (*A*) Design of the very high–density seeding-induced spatial confinement strategy and establishment of HepaRG (RG)-derived cell lines, including HepaSL (SL; SL_0 indicates the cells just after 20-h spatial confinement), HepaRP (RP; RP_0 just after 20-h spatial confinement), and HepaED obtained after sequential exposure to endocrine factors allowing the early endoderm specification stage (End.) to be reached after 5 d, followed by a prehepatogenesis stage after a further 3-d exposure to activin A (ED). (*B*) Phase-contrast micrographs (bar: 180 µm) showing HepaSL cells switched to RG medium with corticoids and subjected (or not) to very high density. Images were taken at confluence (14 d or 18 d) and after an additional 14 d (day 28) or 18 d (day 36) in the presence of 1.5% DMSO. It can be observed that HepaSL cells completed the hepatocyte differentiation program in the presence of corticoids only when a 20-h spatial confinement at very high density was applied to obtain HepaRP cells (see yellow arrows that indicate appearance of hepatocyte colonies). (*C*) Representative karyograms, T+C staining (telomeres in red; centromeres in green), and M-FISH images for HepaRG, HepaSL, and HepaRP cells at indicated passages. The nature and frequency of chromosomal aberrations allowed building a detailed karyotype evolutionary tree that shows how shape stress produced chromosomal variation and clone diversification. Zoomed-in images were generated based on TC+M-FISH results. (*D*) Overview of the proteome in the three cell lines (N = 3 to 4 per cell line). Differences are shown as heatmaps of all and differentially expressed (DE) proteins that were produced by hierarchical clustering from the intensity-based label-free quantification approach (nanoLC-MS/MS). Signal values between biological replicates from the different cell lines were successfully discriminated (yellow, black, and blue boxes represent down-regulated, intermediate, and up-regulated proteins, respectively).

receptor inhibitor SB431542. In this way, hepatoblastic cells were obtained before applying the conditions usually required for HepaRG hepatocyte differentiation or cholangiocyte production (*SI Appendix*, Fig. S2*D*). HepaSL cells were indeed able, with great efficiency, to reach the early endoderm stage (End.) and then differentiate into bipotent hepatoblasts, in a manner similar to what has been reported for human ESCs. Bipotent hepatoblasts refer to common progenitors of hepatocytes and cholangiocytes, also characterized by the expression of several liver-specific markers (35) and described during liver organogenesis (36). From these

data, we also postulate that HepaSL might be able to differentiate as well into cells with endodermal properties such as pancreatic or intestinal cells.

Furthermore, HepaSL cells directly seeded at the usual low density in the presence of corticoids did not succeed to complete hepatocyte maturation (Fig. 1*B*). In fact, successful reprogramming of HepaSL cells (taken at P4, P9, or P12 in this work) into hepatoblastic and then mature, well-polarized and functional hepatocyte-like cells surrounded by epithelial cells, could only be obtained by application of a 20-h very high–density stress (vHD, 4.3×10^5 cells/cm^2) before reseeding under proliferating conditions at the usual low density in the presence of corticoids (Fig. 1*B* and *SI Appendix*, Figs. S2 *B* and *C* and S3). Remarkably, a stable line of reprogrammed cells, the HepaRP line, was successfully established from HepaSL cells following spatial confinement for 20 h at very high density (cell fraction harvested as HepaRP$_0$) by repeated expansion of cells arrived at subconfluence (*SI Appendix*, Fig. S3). Thus, HepaRP cells appear capable of transdifferentiating as HepaRG cells do (31), with an expansion capacity and stability potential for at least 20 to 22 passages corresponding to 64 to 65 PDs in total (*SI Appendix*, Fig. S1*A*). Thus, the conversion of HepaSL cells to HepaRP progenitors by a 20-h physical stress at very high cell density restored for the second time the maximum number of potential DNA replications or cell divisions that characterizes the original HepaRG cell line, again delaying progression to a more aggressive cancerous state, i.e., entry into the transformation crisis. This double bypass of the Hayflick limit strongly suggests that high cellularity in a restricted space, possibly involving compressive forces, induces processes that act as barriers against transformation.

Since the arrest of cell divisions when reaching replicative senescence has been associated with the accumulation of DNA aberrations (37), we postulated that the HepaRG-derived cell lines we established might have escaped, at least in part, the accumulation of genomic aberrations. Using telomere and centromere staining followed by the M-FISH technique, karyotyping showed that the general profile of the original HepaRG cells was preserved in HepaSL and HepaRP cells (Fig. 1*C*). The chr 7 trisomy, already known for HepaRG cells, was also present in HepaSL cells. Intriguingly, we show the presence of a dicentric chromosome (chr) resulting from the abnormal fusion of the long arm of chr22 to the long arm of chr12 (dic(12;22)(p10;p10), in 100% of cells in the different lines, whereas this aberration had previously been described as a translocation with the monosomy of chr22 (24). Further analysis of karyotype profiles revealed that HepaRP cells were divided into two major populations. Cells from the minority population (35% of HepaRP cells) appeared similar to HepaRG cells, whereas cells from the majority population (65% of HepaRP cells) showed particular chromosomal aberrations within proliferating clones, including the presence of only a supernumerary ring chr 7 with centromere breakpoints allowing restoration of the diploid karyotype profile (Fig. 1*C*). This great improvement in the chromosomal quality of cells in the majority HepaRP population could be very beneficial for pharmacovigilance and drug safety studies. It is possible to take advantage of the clonality of HepaRP cells to select the most stable clones, which should make it possible to establish in the future a series of cell lines with novel properties.

At the proteome level of the HepaRG-derived cell lines established here (see details in Dataset S1), unbiased analysis highlighted that the main changes involved processes linked to the main functions of differentiated liver cells (e.g., fuel metabolism, detoxification, plasma protein synthesis; see details in *SI Appendix*, Fig. S4). Hierarchical clustering analyses performed from either all 3,449 proteins quantified in this study or only the 1,407 proteins that exhibited an ANOVA *P*-value below 0.05 resulted in very similar profiles (Fig. 1*D*). Hence, all different cell groups were successfully distinguished from each other, which indicates low variability between biological replicates. Moreover, protein levels in HepaRG progenitors and HepaRP$_9$ cells formed a larger cluster, which was well distinguished from another one grouping together HepaSL, HepaED, and HepaRP$_0$ cells. This may be indicative of a more or less differentiated state, the detail of which is deciphered below. Triggering mechanical signals (i.e. due to compression) by seeding at very high density therefore appears to be a powerful procedure for obtaining reproducible replicates of stable cell lines.

Very High Density and Corticoids Allow to Direct the Transdifferentiation of Hepatic HepaRG Cells. One of our observations was that HepaSL cells were no longer sensitive to the physical confluence signal, which usually triggers the complete hepatocyte differentiation of HepaRG cells in the presence of corticoids (Fig. 1*B*). This strongly suggested that mechanosignals induced by spatial confinement at very high density in the absence of corticoids had induced properties associated with dedifferentiation in HepaSL cells, distinct from those acting in HepaRG progenitor cells. Thus, dedifferentiated HepaSL cells were expected to express stem-like properties. Accordingly, expression levels of key stemness markers highlighted a stem-like phenotype in HepaSL cells as well as in cells that were harvested after passing the early endodermal stage (HepaED) through sequential endocrine treatment (Fig. 1*A*). Indeed, serpin H1 (SERPINH1), an epithelial-mesenchymal transition (EMT) inducer, and high mobility group protein HMGI-C (HMGA2), a chromatin and genome-associated self-renewal modulator, appeared expressed at higher levels in HepaED cells vs. other cell types (1.2- to 4.4-fold), the lowest expression levels being recorded in HepaRG and HepaRP$_9$ progenitor cells, while the levels in HepaSL and HepaRP$_0$ cells remained intermediary (*SI Appendix*, Fig. S5*A*).

Next, focusing on major markers of pluripotency, we found that the mRNA levels of the Nanog homeobox (*Nanog*) were significantly lower in HepaSL cells and in HepaRG and HepaRP$_9$ progenitors compared to fully differentiated HepaRG cells (–30 to 50%), and lower levels were also seen in HepaRP$_0$ cells, but significance was not reached (Fig. 2*A*). The relative maintenance of *Nanog* and POU domain, class 5, transcription factor 1 (*Oct4*) levels may be linked to the cancer origin of these cells and to the well-preserved plasticity properties essential to performing dedifferentiation or redifferentiation in the 3 lines (31). Transforming growth factor beta-1 protein (TGFB1), a powerful morphogen, was expressed at higher values in HepaED compared to other cell types (*SI Appendix*, Fig. S5*A*), which could be linked to the presence of activin in the medium, used here as an early endocrine differentiation factor. Indeed, activin and TGF-β expression are strongly interacting and regulate each other. These observations suggest that TGFB1 may not be of equal importance for hormonally versus mechanically induced differentiation pathways. During the establishment of HepaSL and HepaRP cells, it could be that TGF-β family members other than TGFB1 were involved to control the tetrameric complex formation between the receptor dimers TGFBR1 and TGFBR2, which is essential for the control of TGF-β signaling. Alternatively, high cellularity itself could have mechanically brought the different members of the heterotetrameric complex of receptors close together, hence triggering their assembly and activation without the need for a particular receptor binding factor (38).

The successful reprogramming of HepaRP$_9$ cells toward expression of a hepatic-like energy metabolism phenotype, close to the original one in HepaRG cells, was confirmed by the

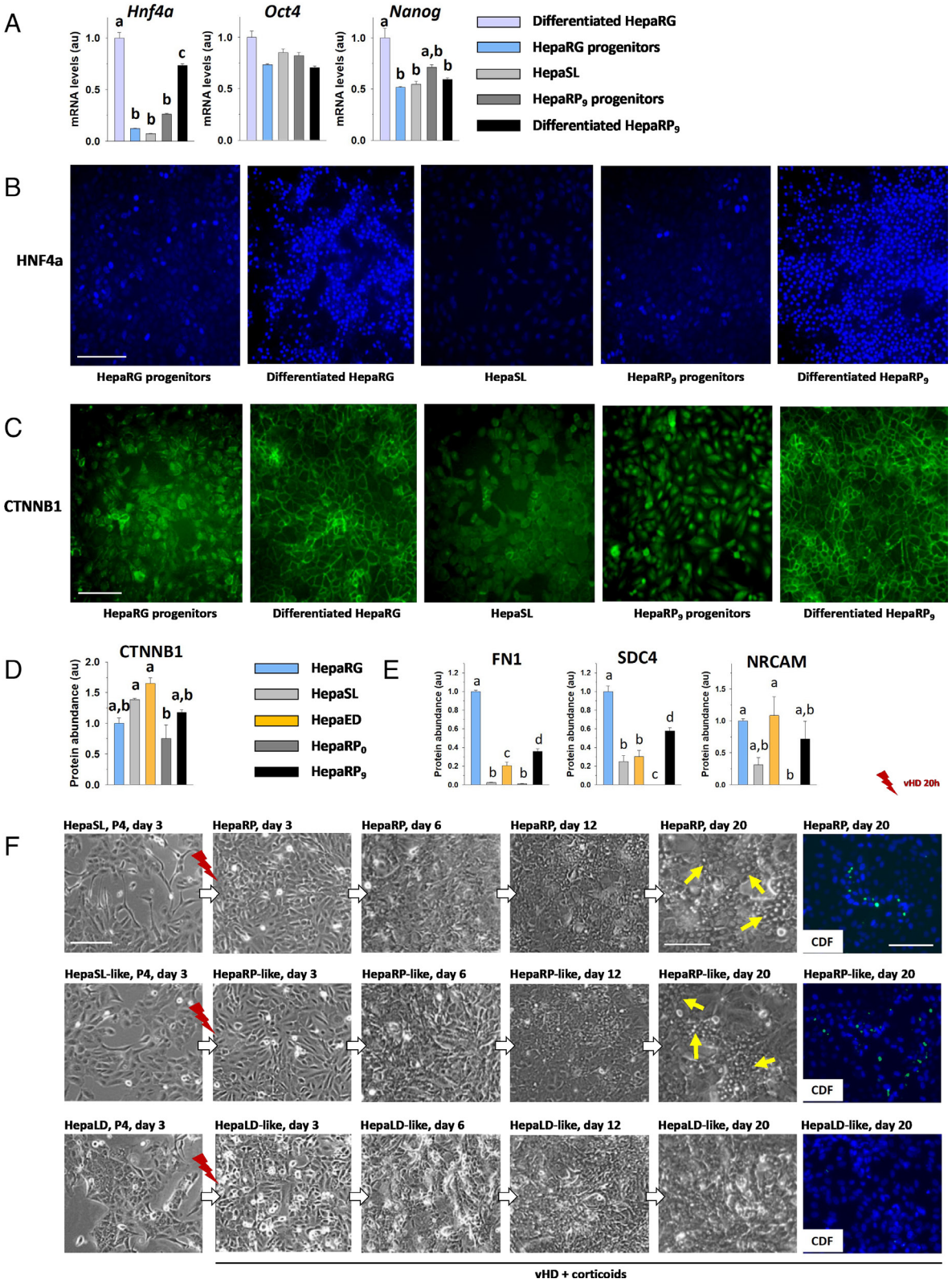

Fig. 2. Differentiation state in HepaRG and HepaRG-derived cell lines. (*A*) mRNA levels for transcription factors known to control the hepatic phenotype (*Hnf4a*, *Oct4*, and *Nanog*) in the same cells as in panels *B* and *C* (p: progenitors, d: differentiated). (*B*) Immunostaining of HNF4a transcription factor in cells from the HepaRG, HepaSL, and HepaRP lines, at day 3 postseeding (progenitors) and at day 25 (differentiated) (bar: 60 µm). (*C* and *D*) CTNNB1 protein abundance and immunostaining (bar: 50 µm). (*E*) Relative abundance of cell surface and cell adhesion factors in HepaRG cells at P13, HepaSL cells at P4 (SL), HepaED cells at the postendoderm stage after exposure to activin A for 3 d, and HepaRP cells collected just after the 20-h confinement constraint ($HepaRP_0$) or at P9 post-physical stress at day 3 post-seeding ($HepaRP_9$). Histobars (mean ± SEM) that do not share the same superscript letter are significantly different (ANOVA and Tukey HSD $P < 0.05$). (*F*) Phase-contrast micrographs (bars: 110 µm) of the HepaSL, HepaSL-like, and HepaLD cells, taken at P4 after seeding on agarose (*SI Appendix*, Fig. S6*B*) and reseeded at very high density (vHD, 4.3×10^5 cells/cm^2) for 20 h to obtain HepaRP, HepaRP-like, and HepaLD-like cells, respectively. As observed for cells reseeded in proliferating conditions at passage 4 on days 3, 6, 12, and 20 postseeding, differentiation into hepatocyte-like cells could be observed for HepaRP and HepaRP-like cells; yellow arrows indicate the appearance of hepatocyte colonies. In contrast, HepaLD-like cells failed to engage in the differentiation process. The property of transport to the bile canaliculi, illustrated by the metabolism of CDFDA and the accumulation of CDF in the bile duct lumen (Bars: 75 µm), was well recovered in HepaRP and HepaRP-like cells, however not in HepaLD-like cells.

expression levels of numerous proteins involved in the main functions of differentiated liver cells (Dataset S1 and *SI Appendix*, Figs. S4 and S5*A*). Indeed, the enzymes involved in energy and fuel metabolism (e.g., GYS1, ALDOC, PCK1/2, PDHA1, CPT1A, HADH, CS, NDUFA6, COX4I1, and ATP5F1A) were all expressed at higher values in HepaRG progenitors and/or especially $HepaRP_9$ cells (twofold on average). The same observation was made for detoxifying enzymes (fourfold on average, e.g., GSTA2, SOD2, and PRDX6), those involved in bile acid metabolism (CYP27A1, HSD17B4), and a similar trend was obtained for the enzymes that are key for ammonium anion elimination (ASS1, GLUL). The production of plasma proteins, another main specific function of the liver, was well represented in our data with the presence of transferrin receptor protein 1 (TFRC), 1.6- to 2.6-fold higher levels in HepaRG cells, and of several apolipoproteins, including APOL2 and APOE. APOE, which is considered a strong marker of the hepatic lineage, was present at very low levels in HepaSL and $HepaRP_0$ cells compared to HepaRG (−82 to 95% lower) and to a lesser extent in HepaED (−42%) and $HepaRP_9$ (−66%) cells.

The aforementioned differentiation markers are controlled by master regulators of the liver phenotype, which we found to be sensitive to the high-density constraint. This is the case for HNF4A, which governs, in response to hormones or specific environmental factors, the coordinated expression of liver-specific genes during the transition from endodermal cells to hepatic progenitor cells. The levels of *Hnf4a* mRNA were 6- to 10-fold higher in $HepaRP_9$ progenitors and HepaRG differentiated cells, compared to HepaRG progenitors, HepaSL, and $HepaRP_0$ cells (Fig. 2*A*). This suggests that HepaRP cells tend to exhibit a higher differentiation state compared to HepaRG cells. Interestingly, immunostaining of HNF4a (Fig. 2*B*) highlighted its nuclear localization only in differentiated HepaRG and $HepaRP_9$ cells, thus confirming that the HepaRP reprogrammed cell line retained the potential to reinitiate complete hepatocyte maturation. Apart from TGF-β (see above), β-catenin (CTNNB1) and Yes-associated proteins are known to modulate the gene expression program in response to high-density stress. As expected from previous work (31), CTNNB1 accumulated in the nucleus and to lesser extent in the cytoplasm of all actively proliferating progenitor cells, whereas the distribution was drastically different in differentiated cells, including $HepaRP_9$, with a clear localization to the plasma membrane (Fig. 2*C*). However, only slight changes in CTNNB1 protein abundance appeared with the lower values recorded for $HepaRP_0$ and the higher ones for HepaED and HepaSL cells (Fig. 2*D*).

Metabolic sensors, responsive to corticoid control of differentiation markers, were also modulated by dedifferentiation and redifferentiation processes. These include insulin receptor substrate 2 (IRS2), which is involved in cytoplasmic signaling of insulin, insulin-like growth factor 1, and other cytokines. IRS2 was detected in HepaRG and $HepaRP_9$ cells but not in HepaSL cells (*SI Appendix*, Fig. S5*B*). Phosphoglycerate dehydrogenase (PHGDH), which promotes the stem cell phenotype in hepatocellular carcinoma (39), was more abundant in HepaED cells compared with all other cells (twofold on average), with the lowest levels in $HepaRP_0$ and $HepaRP_9$ cells (*SI Appendix*, Fig. S5*B*). These variations appear to be consistent with a lower proliferative state in all cells compared to HepaED, and the same trend is expected in the HepaRP line compared to HepaSL cells and HepaRG progenitors. We also noticed that NAD-dependent protein deacylase sirtuin-5 (SIRT5) was expressed in all cell lines, however, at lower levels in nondifferentiated HepaSL cells (−40 to 77%, *SI Appendix*, Fig. S5*B*). This is in accordance with a previous study that reported reduced liver function with decreased glycolytic flux in primary hepatocytes isolated from mice lacking SIRT5 (40). Thus, SIRT5 expression profiles may be involved in the dedifferentiation of HepaRG progenitors into HepaSL cells induced by very high–density spatial stress. It is also interesting to note that SIRT5 expression levels were comparable in $HepaRP_0$ and $HepaRP_9$ cells, which suggests a rapid reinitiation during exposure to the same external physical forces in the presence of corticoids (*SI Appendix*, Fig. S5*B*). Reinitiation of SIRT5 expression also occurred early during the endocrine-induced differentiation program as suggested by its high levels in HepaED cells. FOS B is another important transcription factor involved in the regulation of proliferation, differentiation, and transformation. We observed that high-density stress had induced the expression of FOSB, which accumulates in $HepaRP_0$, while its levels remain below our limit of detection in the other cell types (*SI Appendix*, Fig. S5*B*). Interestingly, overexpression of FOSB was reported during shear stress, another type of environmental force, in osteoblasts in vitro, which promoted the osteogenic differentiation program (41). Here, we hypothesize that FOSB may play a major role in the redirection of HepaSL cells to HepaRP cells reprogrammed into hepatoblasts. Finally, N-myc-down-regulated gene 1 (NDRG1), known to inhibit the EMT (42), was highly expressed in $HepaRP_0$ and $HepaRP_9$ cells compared to HepaRG (twofold) and to the two other cell groups HepaSL and HepaED (4.3-fold on average, *SI Appendix*, Fig. S5*B*), supporting the idea that the HepaRP cell line is strongly engaged in a well-controlled hepatic differentiation process and suggesting that this cell line possesses antiproliferative and anti-invasive properties.

Since the HepaRG-derived cell lines displayed unique properties after seeding at very high density for 20 h, we wanted to further decipher the physical signals potentially at play in the confined cell microenvironment. Indeed, intracellular tensional signals due to cell–substrate and cell–cell interactions are well known to profoundly influence the fate of many cell types, including liver cells (15, 43). However, only a few reports describe the role of high cell density on reversion and maintenance of stem cell properties (21, 44). In our study, the originality was to use a very high density during seeding, in order to inhibit the anchoring of cells with the substrate and thus avoid internal tension forces usually induced by cell adhesion, so that cell roundness was preserved. In perfect agreement, the proteomic results revealed here profound changes in the expression profiles of extracellular matrix proteins in the case of cells subjected to 20-h very high–density stress (Fig. 2*E*, *SI Appendix*, Fig. S4, and Dataset S1). For example, the drastic repression of the levels of fibronectin (FN1), syndecan-4 (SDC4), and neuronal cell adhesion molecule (NRCAM) in HepaSL (−80.7% on average) and $HepaRP_0$ (−99.7% on average) cells could reflect a mechanosignal where very high–cell density led to cells breaking free from matrix attachment via remodeling of genome expression.

Since we could not prejudge whether it is the maintained roundness of cells at very high density, a density-dependent modulation of cell–cell interactions, or a compressive signal due to spatial confinement that played a key role in the processes of dedifferentiation and reinitiation of differentiation, we set up a procedure in which only spatial constraints, possibly triggering compressive forces, were applied by seeding cells on an agarose substrate and we compared the resulting cells with control cells seeded on plastic. We seeded HepaRG progenitor cells on agarose either at low (2.7×10^4 cells/cm^2) or very high (vHD, 4.3×10^5 cells/cm^2) density. The cells did not attach to the agarose support, unlike what they do on plastic, and therefore remained round at all densities (*SI Appendix*, Fig. S6 *A* and *B*). Seeding of HepaRG cells (P13) for 20 h on plastic or agarose without corticoids, either at very high density (vHD) or at low density, was

followed by reseeding under normal proliferative conditions (*SI Appendix*, Fig. S6*B*). After vHD, the cells obtained on agarose (HepaSL-like) closely resembled the control HepaSL cells seeded on plastic from the start of the procedure. These data show that the dedifferentiation process can occur on agarose, i.e., without the internal tension forces usually produced on the matrix by adhesion to the substrate since the cells were not anchored here. Intriguingly, cells obtained without the application of vHD (HepaLD) had distinct properties, presenting homogeneous colonies of epithelioid cells with granular cytoplasm and slow growth activity during the three first passages (*SI Appendix*, Fig. S6*B*). HepaLD cells, which remained round and formed free aggregates in an unconfined environment for 20 h, therefore, seem unable to dedifferentiate. We next were interested in the ability of the three cell lines established here to reinitiate a differentiation program. The HepaSL, HepaSL-like, and HepaLD cells (taken at P4) were reseeded, either directly in proliferative conditions with corticoids, i.e., without application of very high–density stress signal (*SI Appendix*, Fig. S6*C*), or submitted to vHD in the presence of corticoids before the proliferative conditions were applied (Fig. 2*F*). After vHD, while proliferation activity appeared very similar for all cells, their ability to reset differentiation at confluence was markedly different. Indeed, contrary to control HepaRP cells and HepaRP-like cells (originating from the HepaSL-like line), alterations in the cell growth pattern were observed for HepaLD-like cells (originating from the HepaLD line), such as the piling up of cells, which appeared as disorganized multilayers of cells, unable to form differentiating hepatocyte colonies. In addition, the liver-specific function of transport to the bile canaliculi, observed in HepaRP and HepaRP-like cells, was not detected in HepaLD-like cells (Fig. 2*F*). Overall, these data provide evidence that high-density seeding (vHD) appears to be crucial not only for the establishment of stable stem-like cell lines but also for the induction of redifferentiation of cells of the HepaRP and HepaRP-like lines in the presence of corticoids. Among the various external forces involved during vHD, we think that compressive stress generated under spatial confinement is triggered, although we cannot exclude the possibility for the involvement of other types of external forces. The recently emerged concept of mechanical cell competition stipulates that cell selection/elimination occurs under conditions of high cell density, through the regulation of the balance between senescence and cancer (22, 45). Therefore, we hypothesized that compressive stress at vHD could enhance genomic stability.

Mechanostimulation Enhances Genomic Stability through Chromatin Remodeling and Restoration of DNA Repair Capacity and Telomere Dynamics. Senescence is a permanent cell cycle arrest that limits replicative potential of cells in vitro, and it is a key component of aging in vivo (46). This replicative senescence is often considered an important anticancer mechanism, being probably the first physiological defense against cell transformation by delaying preneoplastic progression to cancer (34). Because replicative senescence is primarily caused by telomere shortening during repeated cell divisions in response to various stimuli such as inflammation and DNA damage (47), we analyzed these chromatin features in HepaRG, stem-like HepaSL, and the reprogrammed HepaRP cells that have escaped senescence and exhibit enhanced chromosomal quality.

Our data reveal that the cell lines established here displayed the classical features of permanently dividing cells, at least with respect to the passages studied. Indeed, changes characteristic of replicative senescence, such as the activation of the p16-Rb and/or p53/p21Waf1/Cip1 pathways (48), were not detected. The levels of retinoblastoma-associated protein (RB1) tended only to diminish in $HepaRP_9$ vs HepaRG, while those of P21 (CDKN1A) exhibited stable levels in the HepaSL and $HepaRP_9$ compared to HepaRG (Fig. 3*A*). Tumor protein p53-inducible protein 11 (TP53I11), which contributes to p53-dependent cell apoptosis regulation, was expressed at lower levels in HepaSL and HepaED cells vs. other cell types (−35%). The abundance of 14-3-3 protein sigma (SFN), which belongs to a subset of p53 targets which mediate cell cycle arrest and senescence (49), tended to decrease by 25% in HepaSL and dropped significantly by up to 55 to 61% in $HepaRP_0$ and $HepaRP_9$ compared to HepaRG cells. Conversely, the level of cytochrome c (CYCS), a key protein activating caspase-9 and -3, which accelerates apoptosis, was significantly higher in $HepaRP_9$ than in HepaRG (1.5-fold) and HepaSL (2.4-fold). This suggests active apoptosis in the HepaRP cell line. Collectively, these results argue for stable or even reduced expression of senescence markers in the cell lines we established.

We then focused on the dramatic and transient changes that occur in cells after a 20-h spatial constraint ($HepaRP_0$), including the induction of repair mechanisms and other molecular events that could enhance chromosome quality, all of which contribute to making the transdifferentiation process possible. We observed changes due to the very high density of cells, which converge to indicate a bypass of senescence and thus an increase in lifespan (Fig. 3*A*), including a sharp decrease in the abundance of cyclin-dependent kinase inhibitor 1 (CDKN1A or p21, by 93 to 95%), growth arrest and DNA damage–inducible proteins–interacting protein 1 (GADD45GIP1, by 29 to 55% and thrombospondin-1 (THBS1, by 83 to 94%), one of the soluble factors known as senescence-associated secretory proteins (50), while the level of FOSB rose at the same time (Fig. 2*C*). Concomitantly, $HepaRP_0$ cells exhibited an increase in the expression levels of proteins involved in protective mechanisms like the unfolded protein response (UPR), as shown previously for nucleus pulposus cells of the intervertebral disc (51). Notably, the abundance of translocating chain-associated membrane protein 1 (TRAM1) was higher (twofold) in $HepaRP_0$ cells compared to all other cells except HepaED (Fig. 3*A*). Similar expression profiles were recorded for other important factors (see details in Dataset S1), including other ER stress–related factors (SEC61B, FBXO2) and many proteins of the ubiquitin–proteasome system (e.g., UBA6, UBA1, UBE2K, UBE2L3, CBL, PSMB1, PSMD2, PSMD3, PSMD11, PSMD13, PSMC1, PSMC2, and PSME1). In the case ER stress becomes too severe, the UPR can activate unique pathways that lead to cell death through apoptosis. Thus, the pro-apoptotic factor BH3–interacting domain death agonist (BID) showed a tendency to be more abundant in HepaSL cells compared to HepaRG progenitors (twofold), significance being reached for the 2.7-fold increase in $HepaRP_0$ cells, while BID levels appeared intermediary in $HepaRP_9$ cells (Fig. 3*A*), and similar expression profiles were recorded for other proteins that play a role in apoptosis (BAD, AIFM1, CYCS; Dataset S1). These data suggest that the cells that are not able to cope with the very high–density stress may be eliminated. In addition, autophagy has emerged as another important protective mechanism during ER stress (52) likely involved in this phenomenon during cell confinement. Indeed, sequestosome-1 (SQSTM1) was significantly (1.6-fold) more abundant in HepaSL and HepaED than other cell types where the levels remained essentially comparable (Fig. 3*A*). We also noticed that the levels of cathepsin L (CTSL) were drastically lower in $HepaRP_0$ cells compared to the other cells (−79%). Together, these stress features may partly explain that no rogue cells were observed in $HepaRP_9$ cells from karyotyping studies, albeit few of them were seen in HepaRG cell preparations (Figs. 1*C* and 3*A*). Finally, a group of proteins higher expressed in $HepaRP_0$ cells could contribute to repress the expression of oxidative stress–related genes. For example, the abundance of plasminogen activator inhibitor 2 (SERPINB2), which contributes to

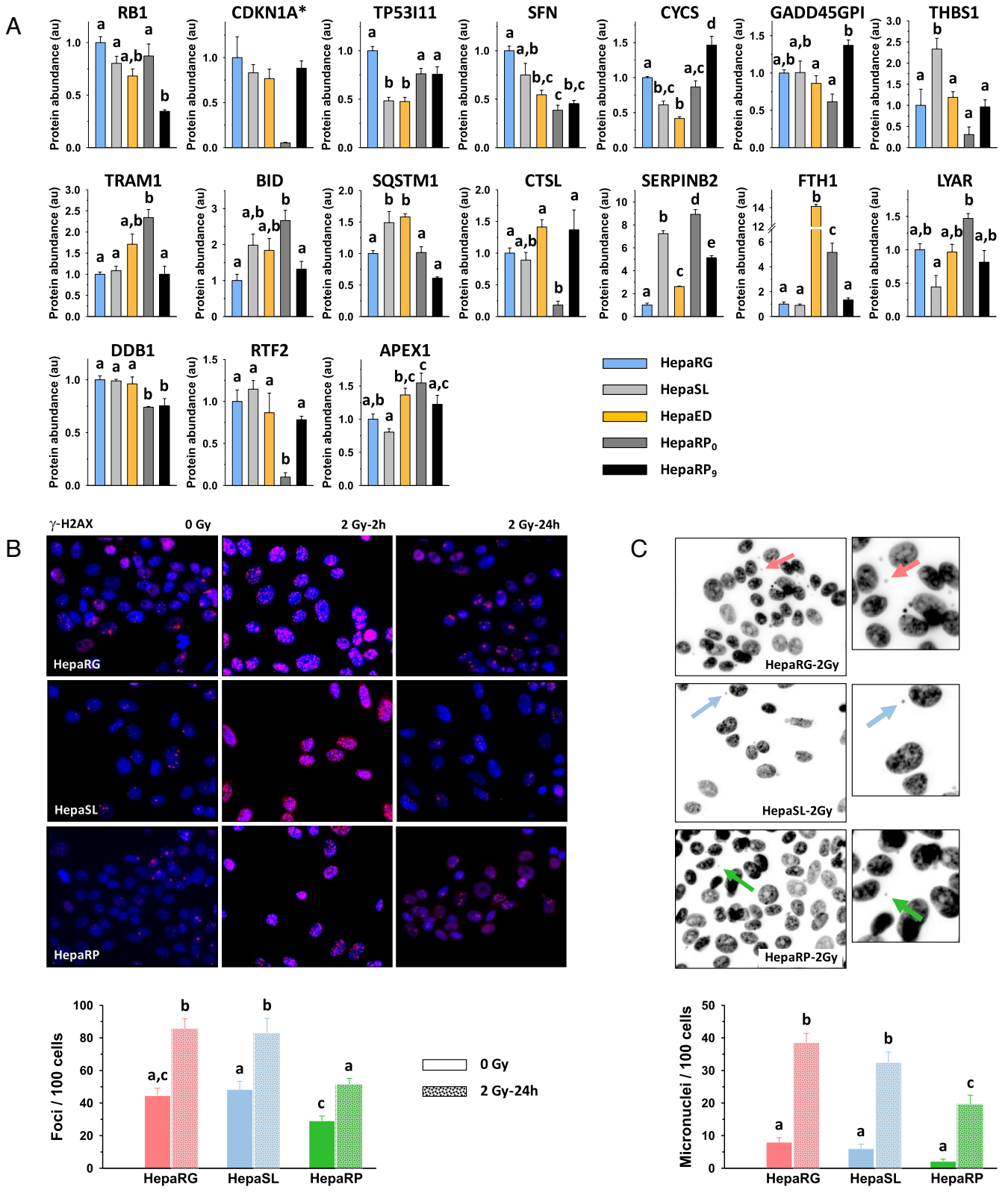

Fig. 3. DNA protection markers and response of HepaRG and HepaRG-derived cells to irradiation. (*A*) Relative abundance of key markers for cells as described in Fig. 2*E*. (*B*) Immunostaining of phosphorylated (pS139) histone H2AX (γ-H2AX, red signal) in cells before (0 Gy) and 2 h and 24 h after 2 Gy X-ray exposure (2 Gy-2h and 2 Gy-24h). γ-H2AX foci (frequency normalized to 100 cells) were quantified before and 24 h after irradiation. (*C*) Micronuclei (frequency normalized to 100 cells), before and 24 h after irradiation. Histobars (mean ± SEM) that do not share the same superscript letter are significantly different (ANOVA and Tukey HSD $P < 0.05$). * indicates that the minimum number of determinations was not reached in one of the cell lines to be able to perform relevant statistical tests, but the trends obviously remain valid.

protect cells from oxidative DNA damages (53), was significantly higher than in HepaRG progenitors (ninefold), HepaSL cells (threefold), and HepaRP9 cells (1.7-fold), the levels in HepaSL and HepaRP$_9$ remaining significantly 7- and 5-fold higher than that in HepaRG cells, respectively. Ferritin heavy chain (FTH1), which is able to effectively control redox homeostasis, was expressed at the

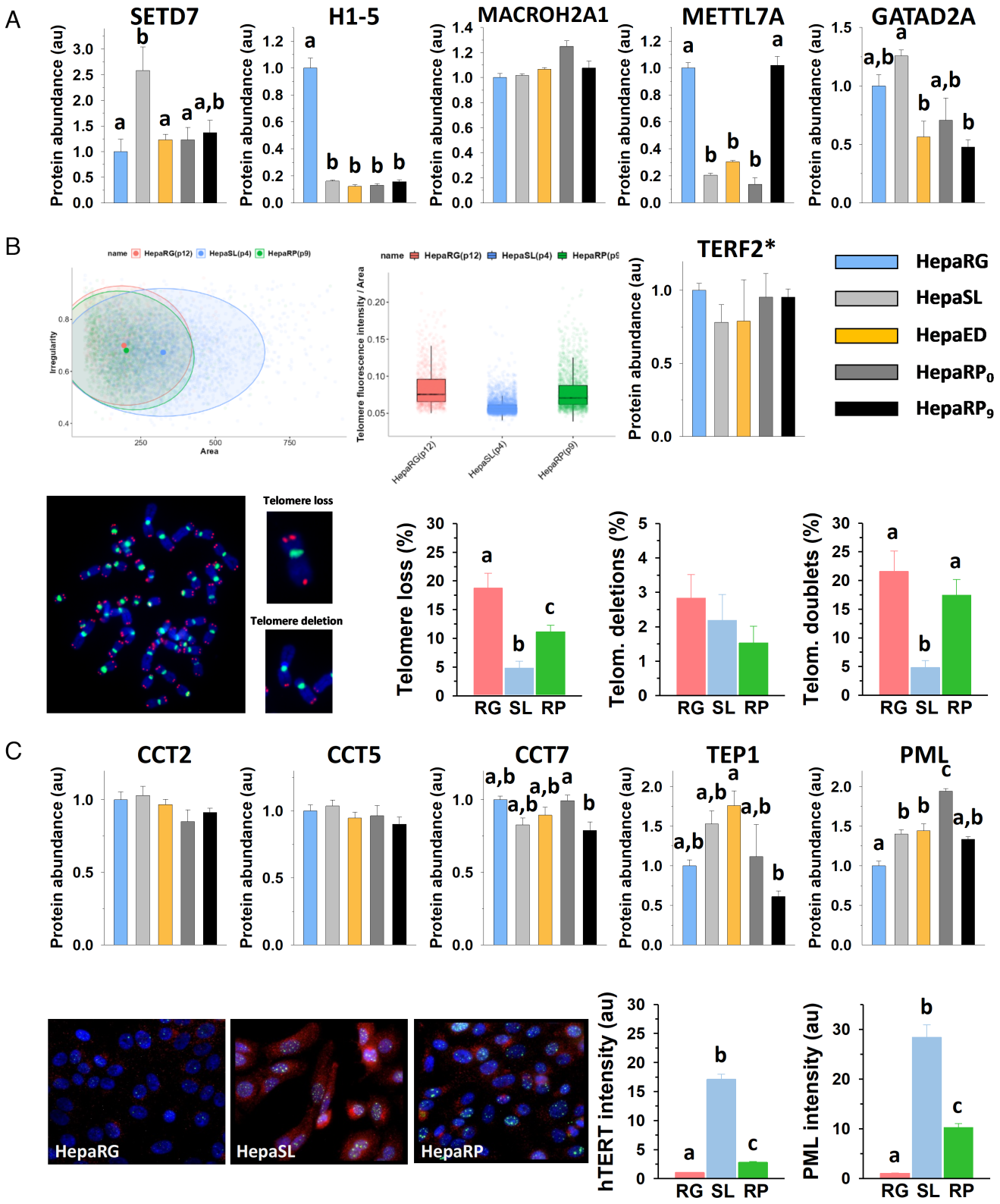

Fig. 4. Chromatin-related markers and telomere dynamics in HepaRG and HepaRG-derived cell lines. (*A*) Relative abundance of key markers for cells as described in Fig. 2*E*. (*B*) Size of cell nuclei, length of telomeres, and rate of telomere loss (defined as a signal-free end of one chromatid), deletions (defined as the loss of telomere signals), and doublets (defined as more than one telomere signal for a single arm) in the three main cell lines as well as relative abundance of telomeric repeat-binding factor 2 (TERF2) for cells as described in Fig. 2*E*. (*C*) Relative abundance of key markers for cells as described in Fig. 2*E*, and immunostaining of hTERT (red signal) and protein PML (bright blue signal) with their deduced expression levels in the three main cell lines. Histobars (mean ± SEM) that do not share the same superscript letter are significantly different (ANOVA and Tukey HSD $P < 0.05$). * indicates that the minimum number of determinations was not reached in one of the cell lines to be able to perform relevant statistical tests, but the trends obviously remain valid.

highest level in HepaED cells compared with all other cells (3- to 16-fold) and was more abundant in $HepaRP_0$ than in HepaRG, HepaSL, and $HepaRP_9$ cells (4- to 5-fold) (Fig. 3*A*). The nucleolar LYAR protein was significantly more abundant in $HepaRP_0$ than in HepaSL and $HepaRP_9$ (two to three times), and a same but nonsignificant trend was observed relative to HepaED and HepaRG cells.

Regarding DNA repair mechanisms, high-density stress seems to cause a strong induction. Indeed, DNA-(apurinic or apyrimidinic site) lyase (APEX1), which is the major AP endonuclease initiating base excision repair that ensures genome integrity (54), was more abundant in $HepaRP_0$ cells (1.4-fold on average compared to other cell types), and in a less pronounced manner in $HepaRP_9$ and HepaED cells (Fig. 3*A*). Importantly, a drastic decreased abundance in $HepaRP_0$ compared to $HepaRP_9$ cells (−85%) of homologous RTF2 protein (RTF2), one of the key players in DNA repair (31), and to a lesser extent (−20%) of DNA damage–binding protein 1 (DDB1), known to be involved in repair and in protein degradation events (55), was detected. Kottemann et al. have shown that RTF2, a component of the replisome, must be removed from stalled forks to allow an effective response to replication stress (56). We therefore hypothesize that genome integrity in $HepaRP_0$ cells could be ensured through efficient restart of stalled replication forks via RTF2 removal under very high density–induced spatial confinement. Using γ-H2AX and 53BP1 as markers of DNA double-strand breaks, we could observe that foci levels were markedly higher in HepaRG before and 2 h after X-ray exposure compared to HepaRP cells (1.6-fold), highlighting a higher stability and a higher capacity for DNA repair in the HepaRP line (Fig. 3*B*). Furthermore, DNA repair 24 h after X-ray exposure appeared most efficient in HepaSL and HepaRP cells and was complete after 48 h in HepaSL. It could be that this function is defective in HepaRG but not in HepaSL and HepaRP cells. To evaluate spontaneous and induced DNA damage, we performed micronucleus assays that highlighted a lower frequency in HepaRP cells than in HepaSL (−39 to −65%) and HepaRG (−49 to −74%) cells, suggesting again a higher chromosomal stability in the HepaRP line (Fig. 3*C*). All of these results converge to demonstrate how physical stress can help prevent senescence and restore genome stability, thereby promoting rejuvenation. With such a reduction in spontaneous genotoxic events as well as improved efficiency of DNA repair processes after the application of spatial constraint stress twice, i.e., after two successive resets of the number of cell divisions before the onset of transformation crisis (see above), not only does the HepaRP cell line appear to be a cell system of choice for toxicology-related studies but the very-high density seeding protocol also appears promising for advancing toward the development of potential innovative anticancer strategies.

The changes we describe here could not have occurred without chromatin remodeling, i.e., modification of the chromatin architecture to reprogram gene expression. This is corroborated by the expression profiles of several factors known to modulate the relaxation/condensation state of chromatin and acetylation of histones (Fig. 4*A*). In particular, the expression levels of histone-lysine N-methyltransferase SETD7 (SETD7) were lower in all cells compared to HepaSL cells (−53% on average), those of histone H1.5 (H1-5) in all cells compared to HepaRG progenitors (−85%), and those of core histone macro-H2A.1 (macroH2A1) in all cells compared to HepaRP0 cells (−17% on average). Interestingly, no change was observed for quantified histone deacetylases (HDAC1, HDAC2, HDAC3, HDAC6; Dataset S1). A higher abundance of methyltransferase-like protein 7A (METTL7A) was recorded in both HepaRG and $HepaRP_9$ progenitor cells compared to other cell types (4.6-fold on average, Fig. 4*A*), arguing for its role in hepatic differentiation of these two differentiating cell lines via regulation of the methylation status of specific genes, as it is the case in osteogenic differentiation (57). In comparison with the other cells, low levels of transcriptional repressor p66-α (GATAD2A) were recorded in both HepaED and $HepaRP_9$ cells (−43%), with a similar trend in $HepaRP_0$ cells (Fig. 4*A*). GATAD2A contributes to transcriptional regulation by nucleosome remodeling and histone deacetylation complex NuRD.

To complete our understanding of the control of replicative capacity in HepaRG-derived cells, we next investigated key DNA features. First, we showed that the size of the nucleus is larger in HepaSL cells than in HepaRG and HepaRP cells (Fig. 4*B*), which suggests an alteration in DNA architecture such as chromatin decondensation, which may allow reprogramming of genome expression but weaken the chromosomes. This led us to explore telomere length dynamics, telomere maintenance being an important process to ensure genome stability. All three cell lines (HepaRG, HepaSL, and HepaRP) appeared characterized by short telomeres but with strong differences between the lines, with the telomere length unexpectedly lower in HepaSL and, to a lesser extent, HepaRP cells (Fig. 4*B*). Nevertheless, we could also observe rehomogenization of the cell population regarding telomere length in HepaRP cells and especially HepaSL cells compared to HepaRG cells. This may suggest selection of the most stable cells in very high–density situations. Accordingly, telomere FISH on metaphase spreads (Fig. 4*B*) highlighted a significantly lower rate of telomere loss in HepaRP (−74%) and in HepaSL (−41%) cells compared to HepaRG cells, thus suggesting a lower risk of chromosomal instability via telomere-end-fusion and breakage/fusion/bridge cycles after seeding at very high density, especially in HepaRP cells. Although significance was not reached for telomere deletion, which represents double-strand breaks, a trend for lower values in HepaSL (−23%) and HepaRP (−46%) cells relative to HepaRG cells was seen. In addition, the less frequent occurrence of telomere doublets in HepaSL (−78%) and, to a lower extent, HepaRP (−19%) cells suggests that the shelterin complex function is improved by our procedure. Accordingly, levels of two members of the shelterin complex (TERF2 and TERF2IP) remained stable in all cell lines (Fig. 4*B*).

Concerning the main pathways for telomere maintenance, we first observed stable expression levels for seven components (CCT2, CCT3, CCT4, CCT5, CCT6A, CCT7, and CCT8; Fig. 4*C* and Dataset S1) of the chaperonin-containing T-complex (TRiC), a key molecular chaperone complex in proteostasis that notably mediates the folding of WRAP53/TCAB1, thereby regulating telomere maintenance (58). The expression levels of one key component (TEP1) of the telomerase ribonucleoprotein complex also remained stable (Fig. 4*C*), and the highest levels of telomerase (hTERT), which activation is the primary mechanism for telomere maintenance (59), were highlighted in HepaSL (17-fold) and HepaRP (threefold) compared to HepaRG cells (Fig. 4*C*). This huge activation of telomerase therefore appears to be a powerful mechanism for the acquisition of genomic stability in cells subjected to external physical stress. The same observation was made from immunostaining and proteomics data for protein PML (Fig. 4*C*), which is key in alternative lengthening of telomere pathways (59). Altogether, these results support global reactivation of telomere elongation processes in the HepaSL and HepaRP lines compared to the parental HepaRG line and converge to demonstrate the highly improved stability in the HepaRP cell line.

Conclusion

Physical stress due to spatial confinement created by very high–density seeding appears to induce the dedifferentiation of hepatoma HepaRG cells into stem-like cells and then render them capable of redifferentiating into hepatic progenitors in the presence of corticoids. Deciphering the mechanotransduction mechanisms behind this result will be the subject of future research. However, it is not surprising to postulate the strong impact of the mechanical

environment on the regulation of competitive interactions between cells through very high cell density, including the elimination of loser or abnormal cells through so-called mechanical cell competition (22, 45). In the same vein, beyond expression levels of *Nanog* and *Oct4*, the identification of signaling factors involved in maintenance/recovery of hepatic memory should be performed in future studies. Indeed, our data suggest that distinct pathways are involved when using the endocrine approach to reinitiate hepatic differentiation program in HepaSL cells.

We provide direct evidence that the HepaRG-derived cell lines established here have enhanced genomic stability and delayed progression to a more aggressive cancer state compared to the parental HepaRG cells. This likely involved reversion of major aspects of the replicative senescence process, for which we found key regulatory functions actively contributing to greater efficiency of DNA repair and restoration of telomerase activity. These observations provide insight into how physical stress interferes with genome stability, representing a paradigm for rescuing cellular instability. This strongly suggests that physical stress such as compressive forces from the environment may play a crucial role in protecting against aggressive progression to cancer, as observed with preneoplastic nodules or differentiated HCC (25). The concept of mechanical cell competition therefore would apply to abnormal or tumor cells sensitive to compaction, which would act as a tumor-suppressive mechanism, promoting the elimination of these dangerous cells (45). This opens innovative avenues for the design of effective therapies that would circumvent the problem of genomic instability associated with cancer.

Last, the very high–density seeding protocol proposed here appears a simple, fast, and reproducible method to create HepaRG-derived cell lines, more stable and more actively proliferating than the initial HepaRG cells. To some extent, there are similarities with the rejuvenation process described in hiPS cells from aged human donors when they undergo differentiation into fibroblastic cells (60). Therefore, if it is possible to escape the Hayflick limit, nothing should prevent repeating the dedifferentiation and redifferentiation processes for each derived cell line (of course, before the cells have reached replicative senescence). Exploiting these data could improve and perpetuate worldwide access to HepaRG line cells i) by removing the limitations associated with the single 20-y bank currently available for distribution, ii) by guaranteeing the possibly infinite sustainability of cell production, and iii) by circumventing the limited duration of use of each batch of HepaRG cells thanks to increased replicative activity with genome stability over numerous population doublings. They could also be used to diversify cell properties via the establishment of new cell lines. Overall, high-density seeding, possibly triggering compressive stress, appears very promising for the development of applications with HepaRG-derived cells, a principle that is probably extensible to several other cell types.

Materials and Methods

HepaRG and HepaRG-derived cells (24) were cultured as previously described according to respective experiments (31, 35, 61). Previously reported methods were used for phase-contrast microscopy, imaging, and cell immunostaining (26) as well as karyotyping and cytogenetic analysis (62), mass spectrometry analyses (63, 64), and RT-qPCR analyses (65). The mass spectrometry proteomics data have been deposited to the ProteomeXchange Consortium via the PRIDE (66) partner repository with the dataset identifier PXD036480. The R software environment v3.4.0 (67) was used for statistical analysis. Detailed culture protocols and all the methods and statistics used are described in *SI Appendix, Additional Methods*.

Data, Materials, and Software Availability. Mass spectrometry data have been deposited in PRIDE (PXD036480) (68).

ACKNOWLEDGMENTS. We are grateful to Dr. M. Théry for helpful discussions on external and internal physical forces and to Prof. A. Guillouzo and Dr. A. Van Dorsselaer for critical comments on the manuscript, and to R. Le Guevel for image captures using ImPACcell platform (Université Rennes 1). This research was supported by French Proteomic Infrastructure (ProFI; ANR-10-INSB-08-03). During the tenure of this study, Charlotte Brun was the recipient of a grant from the Ministère Français de l'Enseignement Supérieur, de la Recherche et de l'Innovation.

Author affiliations: [a]Université de Strasbourg, CNRS, Institut Pluridisciplinaire Hubert Curien UMR 7178, Strasbourg F-67000, France; [b]Proteomics French Infrastructure, FR2048, ProFI, Strasbourg F-67000, France; [c]Université de Rennes 1, INSERM U1241, Nutrition, Métabolismes et Cancer, Rennes F-35033, France; [d]Cell Environment DNA Damage R&D, Genopole, Evry F-91058, France; [e]Université de Haute-Alsace, Institut de Recherche en Informatique, Mathématiques, Automatique et Signal, Mulhouse F-68093, France; and [f]Groupe Hospitalier de la Région de Mulhouse et Sud Alsace Mulhouse, Service de génétique, Mulhouse F-68070, France

1. J. M. Llovet *et al.*, Hepatocellular carcinoma. *Nat. Rev. Dis. Primers* **7**, 6 (2021).
2. A. Villanueva, Hepatocellular carcinoma. *N. Engl. J. Med.* **380**, 1450–1462 (2019).
3. S. Boyault *et al.*, Transcriptome classification of HCC is related to gene alterations and to new therapeutic targets. *Hepatology* **45**, 42–52 (2007).
4. S. Rebouissou, J. C. Nault, Advances in molecular classification and precision oncology in hepatocellular carcinoma. *J. Hepatol.* **72**, 215–229 (2020).
5. J. Zucman-Rossi, A. Villanueva, J. C. Nault, J. M. Llovet, Genetic landscape and biomarkers of hepatocellular carcinoma. *Gastroenterology* **149**, 1226–1239.e4 (2015).
6. J. P. Capp, Cancer stem cells: From historical roots to a new perspective. *J. Oncol.* **2019**, 5189232 (2019).
7. H. Mohammadi, E. Sahai, Mechanisms and impact of altered tumour mechanics. *Nat. Cell. Biol.* **20**, 766–774 (2018).
8. M. Z. Jin, W. L. Jin, The updated landscape of tumor microenvironment and drug repurposing. *Signal Transduct. Target. Ther.* **5**, 166 (2020).
9. M. Fane, A. T. Weeraratna, How the ageing microenvironment influences tumour progression. *Nat. Rev. Cancer* **20**, 89–106 (2020).
10. P. A. Janmey, R. T. Miller, Mechanisms of mechanical signaling in development and disease. *J. Cell Sci.* **124**, 9–18 (2011).
11. A. Nagelkerke, J. Bussink, A. E. Rowan, P. N. Span, The mechanical microenvironment in cancer: How physics affects tumours. *Semin. Cancer Biol.* **35**, 62–70 (2015).
12. R. McBeath, D. M. Pirone, C. M. Nelson, K. Bhadriraju, C. S. Chen, Cell shape, cytoskeletal tension, and RhoA regulate stem cell lineage commitment. *Dev. Cell* **6**, 483–495 (2004).
13. K. H. Vining, D. J. Mooney, Mechanical forces direct stem cell behaviour in development and regeneration. *Nat. Rev. Mol. Cell Biol.* **18**, 728–742 (2017).
14. A. J. Steward, D. J. Kelly, Mechanical regulation of mesenchymal stem cell differentiation. *J. Anat.* **227**, 717–731 (2015).
15. R. J. Wade, J. A. Burdick, Engineering ECM signals into biomaterials. *Mater. Today* **15**, 454–459 (2012).
16. F. Martino, A. R. Perestrelo, V. Vinarsky, S. Pagliari, G. Forte, Cellular mechanotransduction: From tension to function. *Front. Physiol.* **9**, 824 (2018).
17. M. Delarue *et al.*, Compressive stress inhibits proliferation in tumor spheroids through a volume limitation. *Biophys. J.* **107**, 1821–1828 (2014).
18. S. Saha, L. Ji, J. J. de Pablo, S. P. Palecek, TGFbeta/Activin/Nodal pathway in inhibition of human embryonic stem cell differentiation by mechanical strain. *Biophys. J.* **94**, 4123–4133 (2008).
19. J. Zhao *et al.*, Mechanical pressure-induced dedifferentiation of myofibroblasts inhibits scarring via SMYD3/ITGBL1 signaling. *Dev. Cell* **58**, 1139–1152.e6 (2023).
20. Y. Li *et al.*, Compression-induced dedifferentiation of adipocytes promotes tumor progression. *Sci. Adv.* **6**, eaax5611 (2020).
21. K. C. Clause, L. J. Liu, K. Tobita, Directed stem cell differentiation: The role of physical forces. *Cell Commun. Adhes.* **17**, 48–54 (2010).
22. N. E. Baker, Emerging mechanisms of cell competition. *Nat. Rev. Genet.* **21**, 683–697 (2020).
23. G. Tascher *et al.*, In-depth proteome analysis highlights HepaRG cells as a versatile cell system surrogate for primary human hepatocytes. *Cells* **8**, 192 (2019).
24. P. Gripon *et al.*, Infection of a human hepatoma cell line by hepatitis B virus. *Proc. Natl. Acad. Sci. U.S.A.* **99**, 15655–15660 (2002).
25. S. Caruso *et al.*, Analysis of liver cancer cell lines identifies agents with likely efficacy against hepatocellular carcinoma and markers of response. *Gastroenterology* **157**, 760–776 (2019).
26. C. Guguen-Guillouzo, A. Guillouzo, Setup and use of HepaRG cells in cholestasis research. *Methods Mol. Biol.* **1981**, 291–312 (2019).
27. C. Guguen-Guillouzo *et al.*, Maintenance and reversibility of active albumin secretion by adult-rat hepatocytes co-cultured with another liver epithelial-cell type. *Exp. Cell Res.* **143**, 47–54 (1983).
28. P. X. Sun *et al.*, Maintenance of primary hepatocyte functions in vitro by inhibiting mechanical tension-induced YAP activation. *Cell Rep.* **29**, 3212–3222 (2019).
29. J. P. Jackson, L. Li, E. D. Chamberlain, H. Wang, S. S. Ferguson, Contextualizing hepatocyte functionality of cryopreserved HepaRG cell cultures. *Drug. Metab. Dispos.* **44**, 1463–1479 (2016).
30. M. Mandon, S. Huet, E. Dubreil, V. Fessard, L. Le Hegarat, Three-dimensional HepaRG spheroids as a liver model to study human genotoxicity in vitro with the single cell gel electrophoresis assay. *Sci. Rep.* **9**, 10548 (2019).
31. V. Cerec *et al.*, Transdifferentiation of hepatocyte-like cells from the human hepatoma HepaRG cell line through bipotent progenitor. *Hepatology* **45**, 957–967 (2007).
32. A. Guillouzo, C. Guguen-Guillouzo, "HepaRG cells as a model for hepatotoxicity studies" in *Stem Cells in Birth Defects Research and Developmental Toxicology*, T. P. Rasmussen, Ed. (John Wiley & Sons Inc., 2018), pp. 309–339.

33. T. Finkel, M. Serrano, M. A. Blasco, The common biology of cancer and ageing. *Nature* **448**, 767–774 (2007).
34. I. A. Rodriguez-Brenes, D. Wodarz, N. L. Komarova, Quantifying replicative senescence as a tumor suppressor pathway and a target for cancer therapy. *Sci. Rep.* **5**, 17660 (2015).
35. F. Sampaziotis *et al.*, Cholangiocytes derived from human induced pluripotent stem cells for disease modeling and drug validation. *Nat. Biotechnol.* **33**, 845–852 (2015).
36. K. Si-Tayeb, F. P. Lemaigre, S. A. Duncan, Organogenesis and development of the liver. *Dev. Cell* **18**, 175–189 (2010).
37. C. B. Harley, A. B. Futcher, C. W. Greider, Telomeres shorten during ageing of human fibroblasts. *Nature* **345**, 458–460 (1990).
38. K. M. Yamada, S. Even-Ram, Integrin regulation of growth factor receptors. *Nat. Cell Biol.* **4**, E75–E76 (2002).
39. Q. Li *et al.*, Kinesin family member 15 promotes cancer stem cell phenotype and malignancy via reactive oxygen species imbalance in hepatocellular carcinoma. *Cancer Lett.* **482**, 112–125 (2020).
40. Y. Nishida *et al.*, SIRT5 regulates both cytosolic and mitochondrial protein malonylation with glycolysis as a major target. *Mol. Cell* **59**, 321–332 (2015).
41. D. Inoue, S. Kido, T. Matsumoto, Transcriptional induction of FosB/DeltaFosB gene by mechanical stress in osteoblasts. *J. Biol. Chem.* **279**, 49795–49803 (2004).
42. L. Mi *et al.*, The metastatic suppressor NDRG1 inhibits EMT, migration and invasion through interaction and promotion of caveolin-1 ubiquitylation in human colorectal cancer cells. *Oncogene* **36**, 4323–4335 (2017).
43. A. Cipitria, M. Salmeron-Sanchez, Mechanotransduction and growth factor signalling to engineer cellular microenvironments. *Adv. Healthc. Mater.* **6**, 1700052 (2017).
44. A. J. Merrell, B. Z. Stanger, Adult cell plasticity in vivo: De-differentiation and transdifferentiation are back in style. *Nat. Rev. Mol. Cell Biol.* **17**, 413–425 (2016).
45. C. Bras-Pereira, E. Moreno, Mechanical cell competition. *Curr. Opin. Cell Biol.* **51**, 15–21 (2018).
46. J. W. Shay, W. E. Wright, Hayflick, his limit, and cellular ageing. *Nat. Rev. Mol. Cell Biol.* **1**, 72–76 (2000).
47. J. Liu, L. Wang, Z. Wang, J. P. Liu, Roles of telomere biology in cell senescence, replicative and chronological agei. *Cells* **8**, 54 (2019).
48. M. Shtutman, B. D. Chang, G. P. Schools, E. V. Broude, Cellular model of p21-induced senescence. *Methods Mol. Biol.* **1534**, 31–39 (2017).
49. D. Lodygin, H. Hermeking, The role of epigenetic inactivation of 14-3-3sigma in human cancer. *Cell Res.* **15**, 237–246 (2005).
50. J. Guillon *et al.*, Regulation of senescence escape by TSP1 and CD47 following chemotherapy treatment. *Cell Death Dis.* **10**, 199 (2019).
51. W. H. Chooi, B. P. Chan, Compression loading-induced stress responses in intervertebral disc cells encapsulated in 3D collagen constructs. *Sci. Rep.* **6**, 26449 (2016).
52. H. O. Rashid, R. K. Yadav, H. R. Kim, H. J. Chae, ER stress: Autophagy induction, inhibition and selection. *Autophagy* **11**, 1956–1977 (2015).
53. H. Majoros *et al.*, SerpinB2 is involved in cellular response upon UV irradiation. *Sci. Rep.* **9**, 2753 (2019).
54. M. L. Fishel, M. R. Kelley, The DNA base excision repair protein Ape1/Ref-1 as a therapeutic and chemopreventive target. *Mol. Aspects Med.* **28**, 375–395 (2007).
55. B. Lovine, M. L. Iannella, M. A. Bevilacqua, Damage-specific DNA binding protein 1 (DDB1): A protein with a wide range of functions. *Int. J. Biochem. Cell Biol.* **43**, 1664–1667 (2011).
56. M. C. Kottemann, B. A. Conti, F. P. Lach, A. Smogorzewska, Removal of RTF2 from stalled replisomes promotes maintenance of genome integrity. *Mol. Cell* **69**, 24–35.e5 (2018).
57. E. Lee, J. Y. Kim, T. K. Kim, S. Y. Park, G. I. Im, Methyltransferase-like protein 7A (METTL7A) promotes cell survival and osteogenic differentiation under metabolic stress. *Cell Death Discov.* **7**, 154 (2021).
58. A. Freund *et al.*, Proteostatic control of telomerase function through TRiC-mediated folding of TCAB1. *Cell* **159**, 1389–1403 (2014).
59. J. Gao, H. A. Pickett, Targeting telomeres: Advances in telomere maintenance mechanism-specific cancer therapies. *Nat. Rev. Cancer* **22**, 515–532 (2022).
60. L. Lapasset *et al.*, Rejuvenating senescent and centenarian human cells by reprogramming through the pluripotent state. *Gene Dev.* **25**, 2248–2253 (2011).
61. M. Thery, L. Blanchoin, Microtubule self-repair. *Curr. Opin. Cell Biol.* **68**, 144–154 (2021).
62. N. Oudrhiri *et al.*, Patient-derived iPSCs reveal evidence of telomere instability and DNA repair deficiency in coats plus syndrome. *Genes (Basel)* **13**, 1395 (2022).
63. J. Cox *et al.*, Accurate proteome-wide label-free quantification by delayed normalization and maximal peptide ratio extraction, termed MaxLFQ. *Mol. Cell Proteomics* **13**, 2513–2526 (2014).
64. C. Carapito *et al.*, MSDA, a proteomics software suite for in-depth Mass Spectrometry Data Analysis using grid computing. *Proteomics* **14**, 1014–1019 (2014).
65. G. Angenard, A. Merdrignac, C. Louis, J. Edeline, C. Coulouarn, Expression of long non-coding RNA ANRIL predicts a poor prognosis in intrahepatic cholangiocarcinoma. *Dig. Liver Dis.* **51**, 1337–1343 (2019).
66. J. A. Vizcaino *et al.*, 2016 update of the PRIDE database and its related tools. *Nucleic Acids Res.* **44**, D447–D456 (2016).
67. R Core Team, R: A Language and Environment for Statistical Computing. (R Foundation for Statistical Computing, Austria, Vienna, 2022), https://www.R-project.org/.
68. F. Bertile, Quantitative LC-MSMS of new hepatoma HepaRG-derived cells obtained using compression forces. Proteomics IDEntifications Database (PRIDE). https://www.ebi.ac.uk/pride/archive/projects/PXD036480. Deposited 2 September 2022.